Supplementary Materials

Hole transport layers regulate polaron formation in perovskite solar cells

Xiaoran Niu[1,#], Peide Zhu[2,#], Ruoying Pang[1], Shuai Wang[1], Jie Zeng[2], Yong Zhang[3,*], Baomin Xu[2], Feng He[1,*]

[1]National Key Laboratory of Laser Spatial Information, Guangdong Provincial Key Laboratory of Aerospace Communication and Networking Technology, Guangdong Provincial Key Laboratory of Integrated Photonic-Electronic Chip, Harbin Institute of Technology (Shenzhen), Shenzhen 518055, Guangdong, China.

[2]Department of Materials Science and Engineering, Southern University of Science and Technology, Shenzhen 518055, Guangdong, China.

[3]Sustainable Energy and Environment Thrust, Function Hub, The Hong Kong University of Science and Technology (Guangzhou), Guangzhou 511400, Guangdong China.

[#]These authors contributed equally to this work.

[*]**Correspondence to:** Prof. Yong Zhang, The Hong Kong University of Science and Technology (Guangzhou), Guangzhou 511400, Guangdong, China. E-mail: yongzhang@hkust-gz.edu.cn; Prof. Feng He, Harbin Institute of Technology (Shenzhen), Shenzhen 518055, Guangdong, China. E-mail: hefeng2020@hit.edu.cn

I. Linear absorption spectrum.

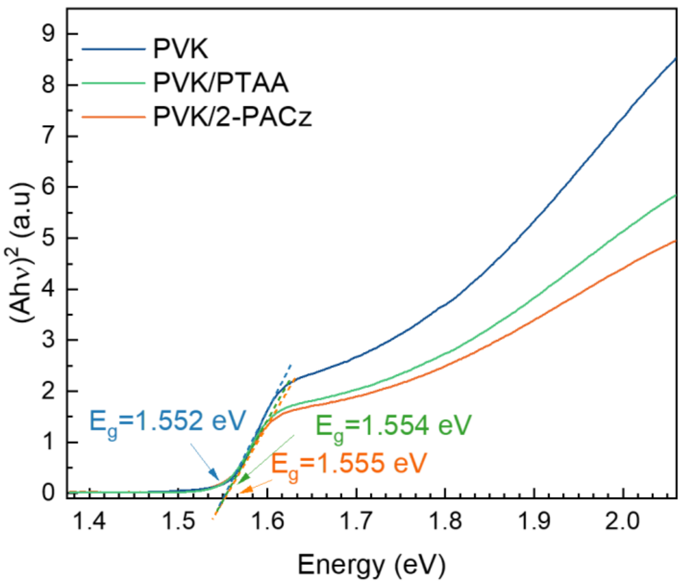

Supplementary Figure 1. Optical bandgap characteristics of perovskite/HTL structures. Tauc plot for pristine PVK, PVK/PTAA and PVK/2-PACz.

Figure S1 presents the Tauc plot for pristine PVK, PVK /PTAA, and PVK /2-PACz. The Tauc plot shows the relationship between the absorption coefficient A and the photon energy E, which for a direct bandgap semiconductor follows the equation: $(Ah\nu)^2 \sim E$.

By fitting a linear equation to the linear portion of the plot and extrapolating the line to intercept the x-axis, the optical bandgap values for the three samples were obtained: 1.552 eV for pristine perovskite, 1.554 eV for perovskite/PTAA, and 1.555 eV for perovskite/2-PACz.

II. TA spectra at various delay times and pump fluences.

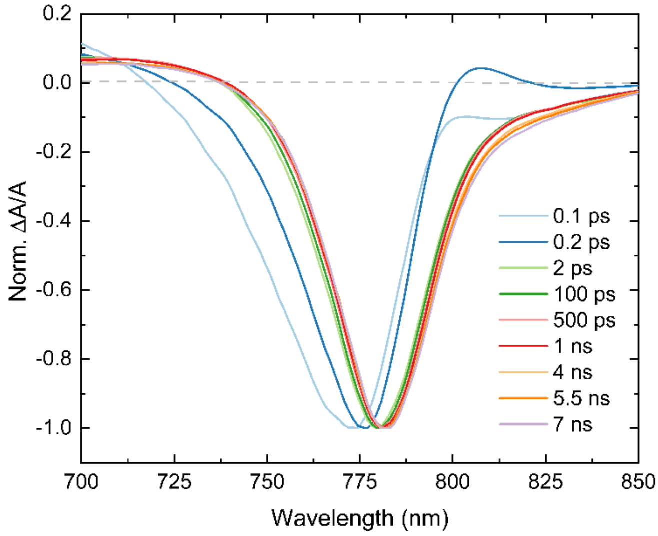

Supplementary Figure 2. Ultrafast spectral evolution of pristine PVK. Normalized TA spectra of pristine PVK at the indicated delay time after excitation at 660 nm at 4.5 μJ/cm^2. The spectra show a clear redshift of the ground-state bleach peak as the delay time increases, reflecting dynamic band-edge relaxation.

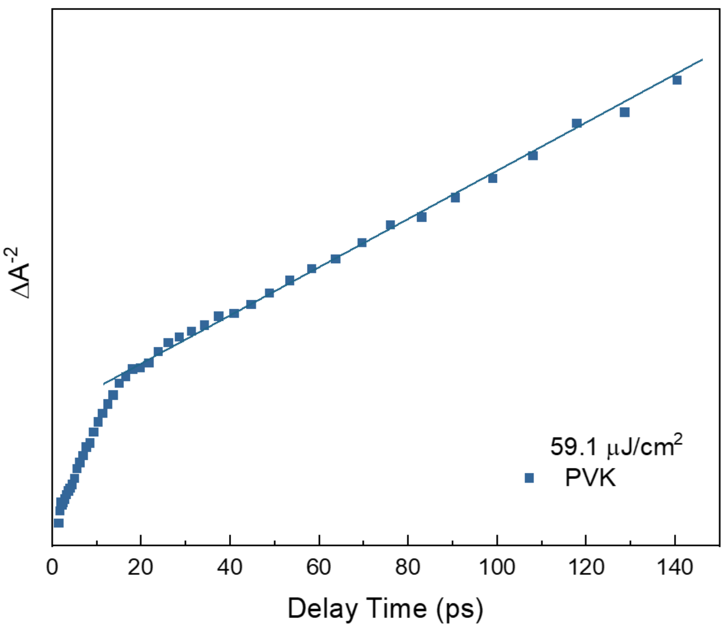

Supplementary Figure 3. Auger-dominated decay dynamics in pristine PVK at high fluence. ΔA^{-2} as a function of time at GSB1 in the TA kinetics for pristine PVK, at a fluence of 59.1 μJ/cm^2. The straight line represents the dominant Auger recombination process occurring after ~15 ps.

III. Decay-associated spectra.

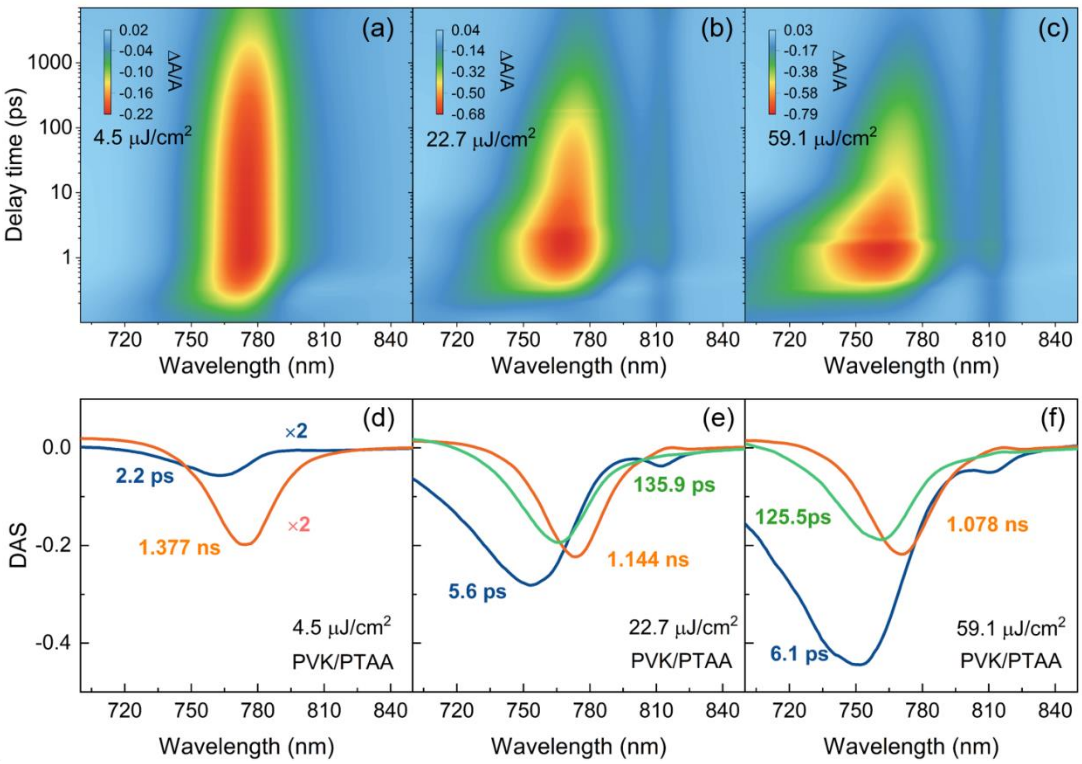

Supplementary Figure 4. Fluence-dependent TAS for PVK/PTAA. (a) TA spectra of pristine PVK/PTAA thin films excited at 660 nm pump at fluences of (a) 4.5 μJ/cm^2, (b) 22.7 μJ/cm^2, and (c) 59.1 μJ/cm^2, along with their corresponding decay-associated spectra (DAS) obtained from global fitting in (d), (e), and (f), respectively.

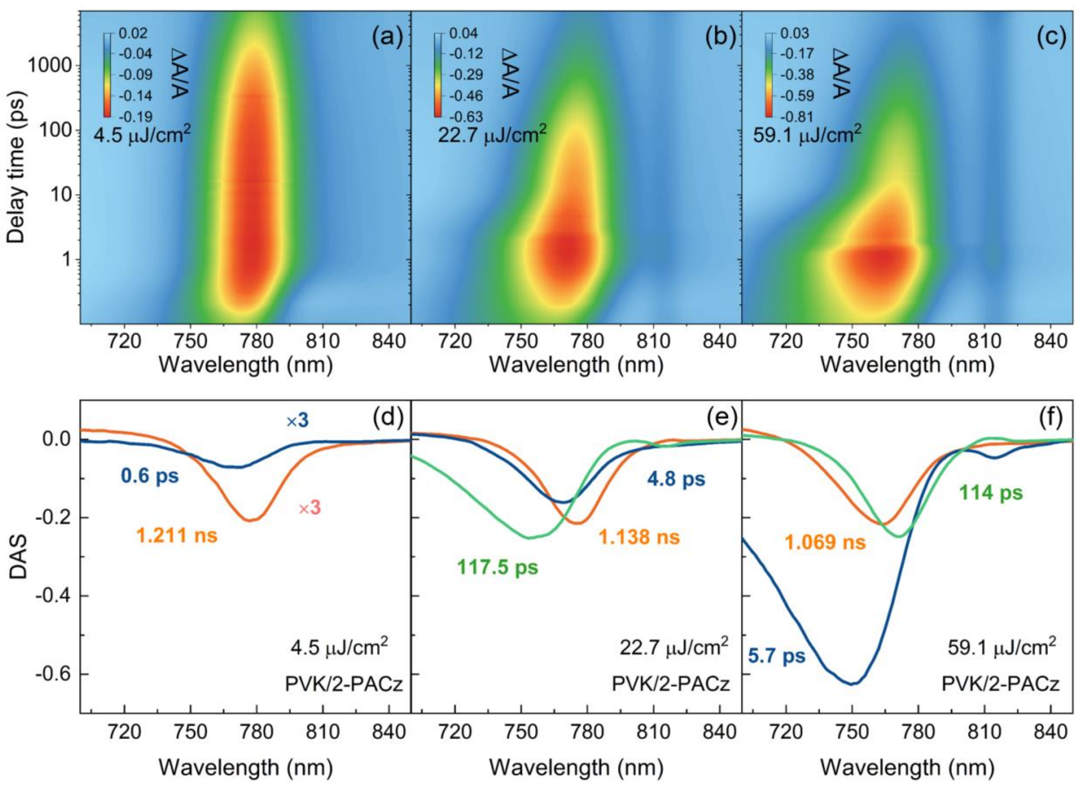

Supplementary Figure 5. Fluence-dependent TAS for PVK/2-PACz. (a) TA spectra of PVK/2-PACz thin films excited at 660 nm pump with fluences of (a) 4.5 μJ/cm^2, (b) 22.7 μJ/cm^2, and (c) 59.1 μJ/cm^2, along with their corresponding DAS obtained from global fitting in (d), (e), and (f), respectively.

IV. TA kinetics of the GSB1 peak.

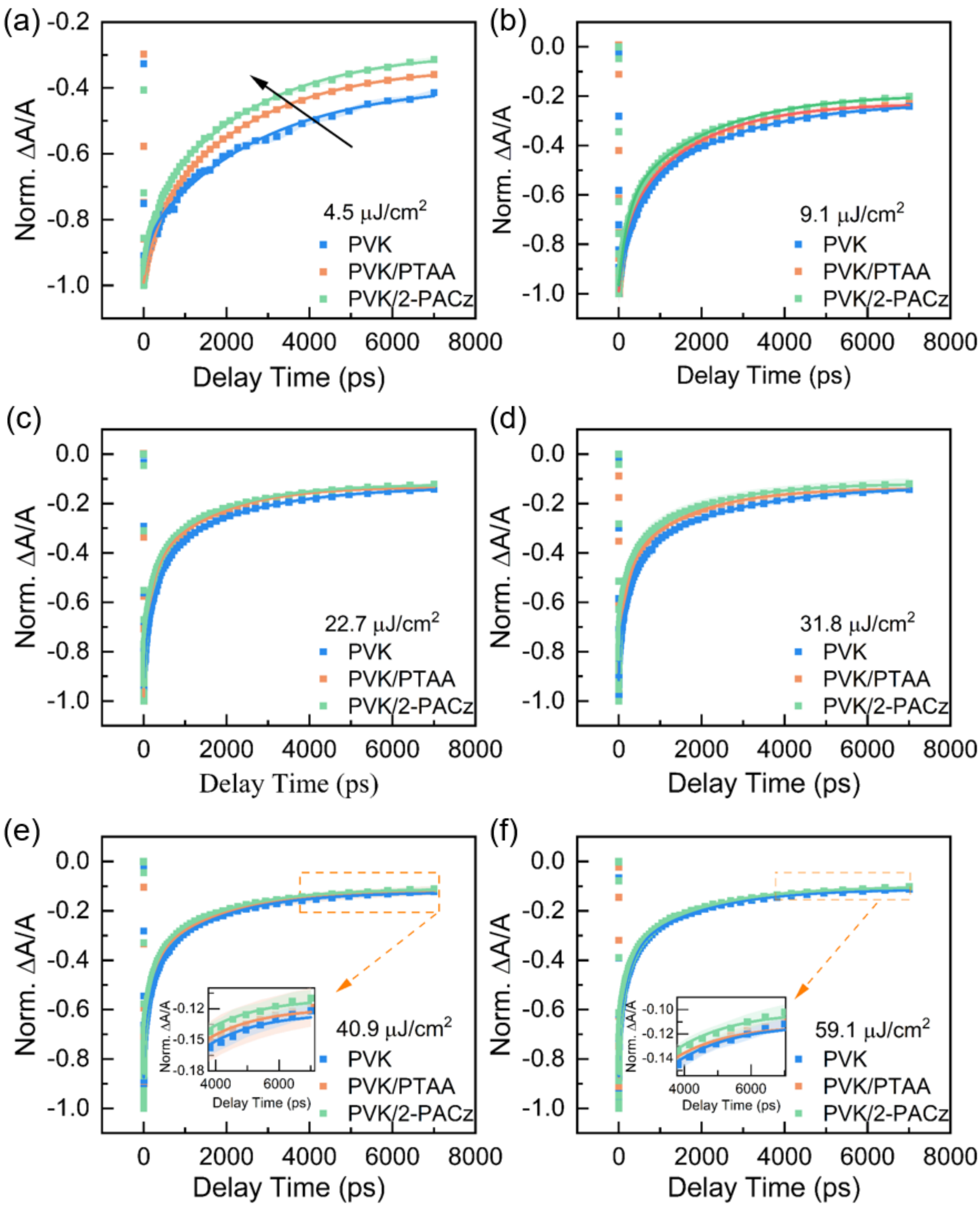

Supplementary Figure 6. Fluence-dependent GSB1 decay kinetics in perovskite films with different HTLs. Normalized TA kinetics of the GSB1 peak for PVK, PVK/PTAA, and PVK/2-PACz under 660 nm excitation with pump fluences of (a) 4.5 μJ/cm^2, (b)

9.1 μJ/cm², (c) 22.7 μJ/cm², (d) 31.8 μJ/cm², (e) 40.9 μJ/cm², and (f) 59.1 μJ/cm². The symbols represent experimental data, shaded regions indicate the standard error, and solid lines show the exponential decay fits. The arrows in panel (a) indicate the direction of faster decay rates.

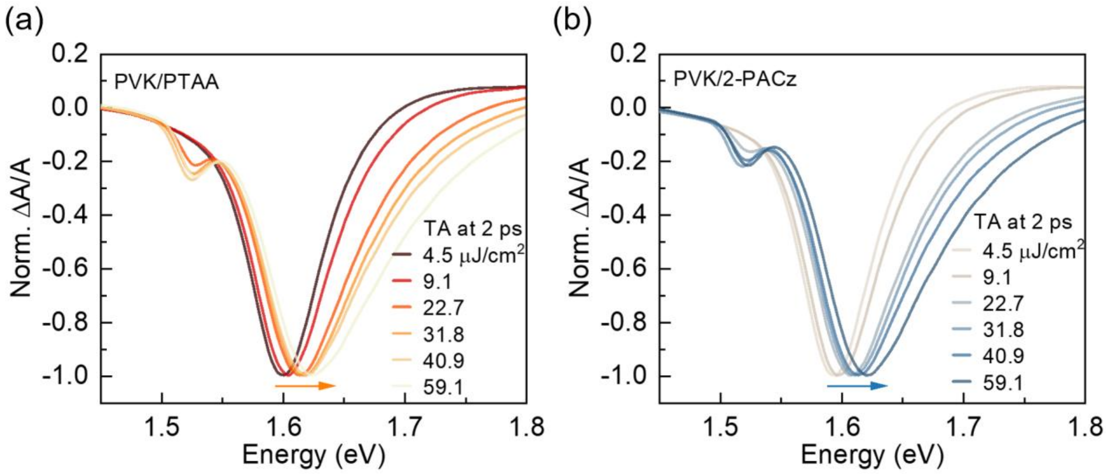

Supplementary Figure 7. Fluence-dependent TAS with HTL. Normalized TA spectra at 2 ps for (a) PVK/PTAA and (b) PVK/2PAC-z film under pump fluences ranging from 4.5 to 59.1 μJ/cm².

V. Device performance.

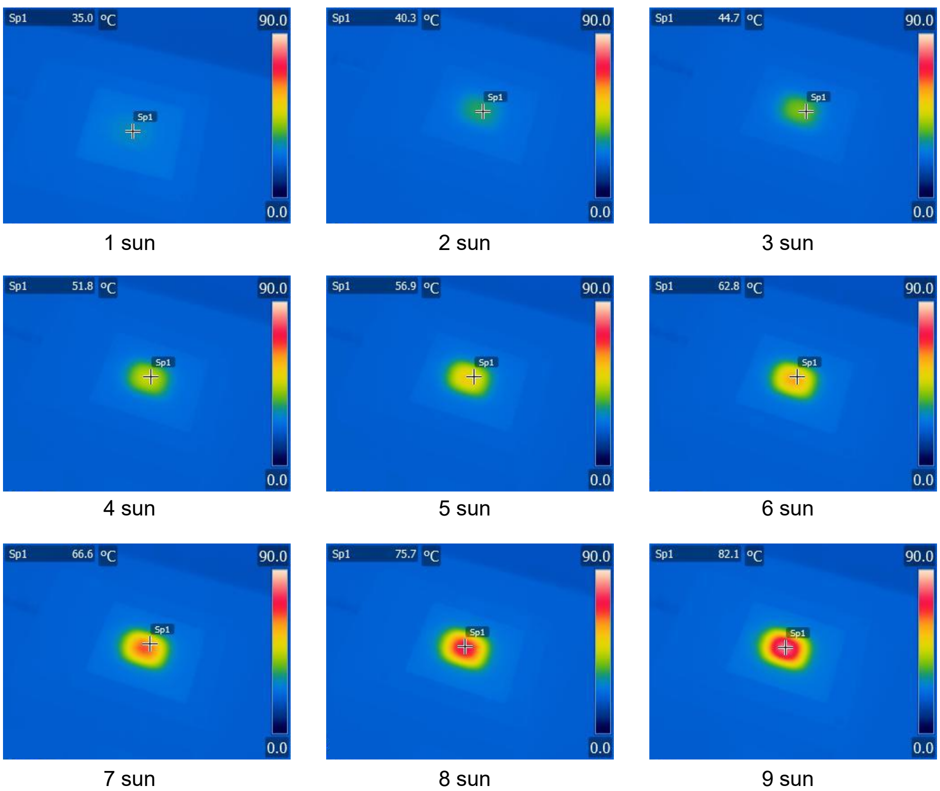

Supplementary Figure 8. Thermal infrared imagery characteristics of the 2-PACz-based device under simulated concentrated AM 1.5 G sunlight at various irradiance levels.

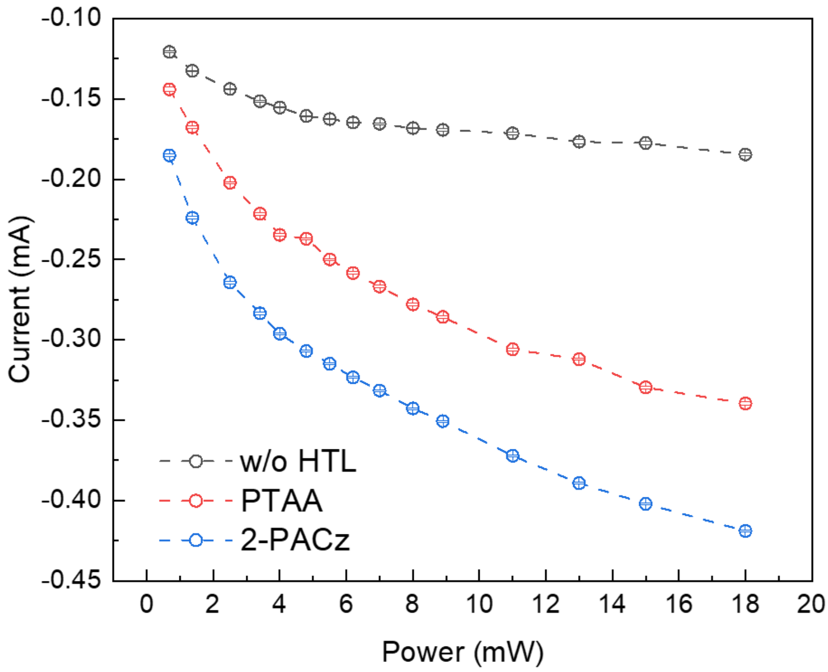

Supplementary Figure 9. Laser power intensity dependent photocurrent of perovskite solar cells measured under 660 nm wavelength laser irradiation, where 17.85 mW corresponds to 59.1 μJ/cm^2.